# Nonlinear Modeling of the Heat Transfer in Loudspeakers

Wolfgang Klippel

Klippel GmbH
Dresden, 01277, Germany
www.klippel.de

**ABSTRACT**

Traditional modeling describes the heat flow in loudspeakers by an equivalent circuit using integrators with different time constants. The parameters of the lumped elements are assumed to be independent of the amplitude of the signal. The simple model fails in describing the forced air convection cooling which becomes an effective cooling mechanism if the velocity of the coil and/or the air velocity in the gap becomes high. This paper presents a large-signal model considering the nonlinear interactions between the electro-mechanical and thermal mechanisms. The model and parameters are verified by practical measurements on the drivers. The dominant paths for the heat flow are identified and means for increasing the power handling capacity are discussed.

## 1  Introduction

Transducers have a relatively low efficiency in the conversion of an electric input into mechanical or acoustical output and most of the energy heats up the voice coil. Although some materials can handle high temperatures ( $T_v > 250\ ^o$ C) the heating is one of the most important factor limiting the acoustical output. For driver and system designers all means are welcome that keep the coil temperature below the critical value: Increasing the efficiency reduces primary heating. There are ways to bypass some power around the coil or to improve the cooling of the coil.

Predicting the voice coil temperature is a complex issue because electrical, mechanical and thermal processes in the driver, enclosure and crossover and the properties of the signal have to be considered. A physical model is required which can be fitted to a particular loudspeaker by measuring a few parameters. Such a physical model is not only useful for the analysis and optimization of the heat transfer but also for designing electronic control circuits giving reliable protection against thermal overload.

This paper follows this target. At the beginning the results of the traditional thermal modeling are summarized and the limits are discussed. Later, an extended model is presented and verified by systematic measurements. Finally, a simple technique for measuring the parameters of the nonlinear model is suggested and the application is discussed on  practical examples.

## 2  Glossary of Symbols

The following symbols are used within the paper.

**State Variables:**

$i$      input current at terminals
$u$      voltage at terminals

$x$        voice coil displacement

$v$        velocity of voice coil

$i_2$       current in resistance $R_2$

$P_{Re}$      power dissipated in $R_e$

$P_{R2}=P_{eddy}$        power dissipated in $R_2$

$P_{coil}=P_{Re}+P_{former}$        power dissipated in voice coil and former

$P_g$        power transferred to the pole tips

$P_{mag}$       power transferred to the magnet

$P_{eg}=(1-\alpha)*P_{eddy}$ power transferred to the pole tips due to eddy currents

$P_{con}$      power transferred to the air in the gap due to convection cooling

$P_{tv}$       power transferred to the pole tips from coil

$P_{ta}$       heat **flow** by air convection from air gap to ambience

$P_{tt}$       heat **flow** by air convection from air gap to the coil facing surfaces of the magnet system assembly

$P_{con}=P_{ta}+P_{tt}$      heat **flow** by air convection from voice coil to air gap

$P_g=P_{tv}+P_{tt}$        heat **flow** both by heat conduction and radiation from voice coil as well as air convection in air gap to the voice coil facing surfaces of the magnet system assembly

$P_t$        power dissipated at minimal impedance of the warm driver

$T_v$        temperature of the voice coil

$T_g$        temperature of the pole tips

$T_m$        temperature of the magnet

$T_{vss}$      steady-state temperature of voice coil in thermal equilibrium

$T_{gss}$      steady-state temperature of the pole tips in thermal equilibrium

$T_{mss}$      steady-state temperature of magnet in thermal equilibrium

$\Delta T_v$       increase of voice coil temperature  $\Delta T_v(t) = T_v(t) - T_a$

$\Delta T_g$       increase of temperature of the pole tips  $\Delta T_g(t) = T_g(t) - T_a$

$\Delta T_m$      increase of the temperature of magnet structure and frame $\Delta T_m(t) = T_m(t) - T_a$

$T_a$        temperature of the cold transducer (ambient temperature)

$\Delta T_{gss}=T_{gss}-T_a$   steady-state temperature increase of eddy current carrying regions except voice coil former in thermal equilibrium over ambient temperature

$\Delta T_{mss}=T_{mss}-T_a$   steady-state temperature increase of magnet system assembly in thermal equilibrium over ambient temperature

$\gamma = \gamma_{LF\ flow\ due\ con} + \gamma_{HF\ generation\ due\ eddy} = (P_{con}+P_{eg})/(P_{Re}+P_{R2})$        bypass factor describing the **heat flow** at both low frequencies by convection bypassing heat conduction & radiation and the **heat generated** at high frequencies by eddy currents except in voice coil former in the eddy current carrying regions

## Electromechanical Parameters:

$R_e(T_v)$ electrical voice coil dc-resistance depending on voice coil temperature

$R_e(T_a) = R_e$     electrical voice coil dc-resistance of cold coil

$L_e$      frequency independent part of voice coil inductance

$L_2$      frequency dependent part of voice coil inductance

$R_2$      resistance due to eddy currents

$M_{ms}$    mechanical mass of driver diaphragm assembly including air load and voice coil

$R_{ms}$    mechanical resistance of total-driver losses

$K_{ms}(x)$  mechanical stiffness of driver suspension

$C_{ms}(x) = 1 / K_{ms}(x)$      mechanical compliance of driver suspension

$Bl(x)$   force factor ($Bl$ product)

$F_m(x,i)$ reluctance force

$f_s$      resonance frequency of the mechanical system

$Z_{min}$    minimum of electrical impedance

$\rho_0$      density of air (=1.18 kg /m$^3$)

$c$       speed of sound in air

$R_e(T_a+\Delta T_v(t))=R_e(T_a)*(1+\delta*\Delta T_v(t))$   time and temperature dependent instantaneous electrical dc resistance of voice coil

$Q_{ts}=Q_{ms}//Q_{es}$  total loss factor describing the transducer

$S_D$         mechanical effective projected surface area of cone assembly to ambient air

$Q_{ms}$        mechanical loss factor describing the mechanical part of transducer

$Q_{es}$        electrical loss factor describing the electromagnetic part of transducer

$Z_{min}(T_v)$    temperature dependent minimum electrical impedance of transducer


**Thermal Parameters:**

$R_t$       total thermal resistance of path from coil to ambience $R_t=R_{tv}+R_{tg}+R_{tm}$

$R_{tv}$      thermal resistance of path from coil to pole tips and magnet surface

$R_{tg}$      thermal resistance of path from pole tips to magnet and frame

$R_{tm}$      thermal resistance of path from magnet to ambient air

$C_{tv}$      thermal capacitance of voice coil and voice coil former

$C_{tg}$      thermal capacitance of pole tips and magnet surface close to coil

$C_{tm}$      thermal capacitance of magnet and frame

$R_{tc}(v)$   thermal resistance of path from coil to air in the gap due to convection cooling

$R_{ta}(x)$   thermal resistance of path from air in the gap to ambience due to convection cooling

$R_{tt}(v)$   thermal resistance of path from air in the gap to the magnet structure due to convection cooling

$C_{ta}$      thermal capacitance of enclosed air in convection cooling

$m_{air}$     mass of enclosed air involved in convection cooling

$\alpha$      factor describing the distribution of heat caused by eddy currents on voice coil and magnet

$r_v$      convection cooling parameter considering the cone velocity $r_v=1/(v_{rms}*R_{tc}(v))$

     $= 1/(2*\pi*f*x_{rms}*R_{tc}(v))$

$r_x$      convection cooling parameter considering the effect of cone displacement $r_x=1/(x_{rms}*R_{ta}(x))$

$\delta$      thermal conductivity parameter ($\delta = 0.039$ for copper)

$\tau_v$      time constant of the voice $\tau_v=R_{tv}*C_{tv}$

$\tau_g$      time constant of pole tips $_g=R_{tg}*C_{tg}$

$\tau_m$      time constant of the magnet frame $\tau_m=R_{tm}*C_{tm}$

**Variables used in power test:**

$\Delta T_{on}$      maximal increase of voice coil temperature $\Delta T_v$ during the ON-phase of the power test cycle

$\Delta T_{off}$      increase of voice coil temperature $\Delta T_v$ measured in the OFF-phase of the power test cycle

$t_{on}$      duration of the ON-phase of the power test cycle

$t_{off}$      duration of the OFF-phase of the power test cycle

$t_{tau\_v}$      time in the last OFF-phase when temperature is decayed to $\Delta T_{tau\_v}$

$t_{s\_off}$      time when the last off-phase starts

$t_{start}$      starting time of the measurement

$t_{tau\_v}$      time when the temperature is equal to $\Delta T_{tau\_m}$

$\Delta T_{tau\_m}$      threshold temperature used for assessing $\tau_m$

$\Delta T_{tau\_v}$      threshold temperature used for assessing $\tau_v$

## 3   Linear Modeling

The traditional modeling uses an electromechanical and a separated thermal model as shown in Fig. 1. At lower frequencies where the wavelength is large compared with the geometrical dimensions, the driver can be modeled by lumped elements having a few number of free parameters. In the traditional approach most of the parameters are assumed as constant but only the voice coil resistance $R_e(T_v)$ depends on the instantaneous voice coil temperature $T_v$. Fortunately, the variation of the temperature is relatively slow compared with the lowest frequency component used in the loudspeaker. Thus, the electro-mechanical model is considered as a linear but time-variant system which can be investigated by straightforward tools.

The thermal model describes the relationship between power $P_t$ dissipated into heat and voice coil temperature $T_v$. At very low frequencies close to dc the power $P_t$ would be identical with the power

$$P_{\text{Re}} = R_e(T_v)i^2 \qquad (1)$$

dissipated in the dc voice coil resistance $R_e(T_v)$ depending on the voice coil temperature $T_v$ and the input current $i$ . Button [2] suggested to use instead of $R_e$ the minimal impedance $Z_{min}(T_v)$ in

$$P_t = Z_{\min}(T_v)i^2 \tag{2}$$

to consider the losses caused by eddy currents and magnetization in the pole plate and magnet. Clearly this rating is only precise at one frequency point above the resonance frequency.

The heating of the coil and the heat transfer to the pole pieces, magnet and ambience can be modeled by a equivalent circuit suggested by Chapman [4] and shown in Fig. 2. This model is more precise and more intuitive than the traditional model using a cascade of parallel RC-integrators [1] - [3]. The potential across the thermal capacitance $C_{tv}$ gives the increase of voice coil temperature $\Delta T_v(t) = T_v(t) - T_a$ with respect to the ambient temperature $T_a$. At the beginning of the heating all input power $P_t$ will flow into the capacitor $C_{tv}$. With rising voice coil temperature $\Delta T_v$ more and more power $P_g$ will be transferred via the thermal resistance $R_{tv}$ to the pole tips having a thermal capacitance $C_{tg}$. With increasing temperature $\Delta T_g(t) = T_g(t) - T_a$ across the capacitor $C_{tg}$ the power $P_{mag}$ is transferred via the thermal resistance $R_{tg}$ to the magnet and frame having the thermal capacitance $C_{tm}$. When the temperature $\Delta T_m(t) = T_m(t) - T_a$ across the capacitor $C_{tm}$ becomes greater zero then some of power is transferred via resistance $R_{tm}$ to the ambience. This model can easily be extended to consider the heating of the air inside a small sealed enclosure as suggested by Behler [5].

## 3.1   Steady-State Behavior

If a stimulus with constant power $P_t$ is applied to the driver, the thermal system will go into a thermal equilibrium eventually. Since no heat flows in or out of capacitors $C_{tv}$, $C_{tg}$ and $C_{tm}$ the thermal resistances $R_{tv}$, $R_{tg}$, $R_{tm}$ determine the steady-state voice coil temperature

$$\Delta T_{vss} = \left(R_{tv} + R_{tg} + R_{tm}\right)P_t = R_t P_t , \tag{3}$$

steady-state pole temperature

$$\Delta T_{gss} = \left(R_{tg} + R_{tm}\right)P_t \tag{4}$$

and the steady-state magnet temperature

$$\Delta T_{mss} = R_{tm}P_t . \tag{5}$$

## 3.2   Linear Dynamics

Varying the input power $P_t$ and observing the temperature $\Delta T_v(t)$, $\Delta T_g(t)$ and $\Delta T_m(t)$ versus time $t$ reveals the effect of the thermal capacities $C_{tv}$, $C_{tg}$ and $C_{tm}$.

After switching on the input power $P_t = P_{on}$ at the time $t = 0$ the temperature $\Delta T_v$ of the voice coil

$$\Delta T_v(t) = \Delta T_{vss} - T_1 e^{-t/\tau_v} - T_2 e^{-t/\tau_p} - T_3 e^{-t/\tau_m} \tag{6}$$

increases by an exponential function (step response) to the steady-state temperature $\Delta T_{vss}$. If the time constants satisfy $\tau_v \ll \tau_g \ll \tau_m$ the parameters of Eq. (6) may be approximated by steady state temperatures

$$T_1 \approx \Delta T_{vss} - \Delta T_{gss}, \tag{7}$$

$$T_2 \approx \Delta T_{gss} - \Delta T_{mss}, \tag{8}$$

$$T_3 \approx \Delta T_{mss} \tag{9}$$

and the time constants of the voice coil

$$\tau_v \approx R_{tv} C_{tv}, \tag{10}$$

the pole piece

$$\tau_g \approx R_{tg} C_{tg} \tag{11}$$

and the magnet

$$\tau_m = R_{tm} C_{tm}. \tag{12}$$

## 3.3   Thermal Power Compression

The increase of the voice coil temperature $\Delta T_v$ has an influence on both the electro-mechanical and the thermal model. Since the temperature $T_v$ reduces the half-space efficiency of the driver in the passband defined by

$$\eta_0(T_v) = \frac{P_a}{P_t} = \frac{\rho_0}{2\pi c} \frac{(Bl)^2}{R_e(T_v)} \frac{S_D^2}{M_{ms}^2} \tag{13}$$

and the input power $P_t$ defined by Eq. (2), there is a natural compression effect in the sound pressure output and in the state variables  displacement, velocity and voice coil temperature.

The thermal coefficient of conductivity $\delta$ describes the relationship between voice coil temperature and voice coil resistance $R_e$

$$R_e(T_A + \Delta T_v) = R_e(T_A)(1 + \delta \Delta T_v) \tag{14}$$

where $\delta = 0.0393$ K$^{-1}$ is valid for copper and $\delta = 0.0377$ K$^{-1}$ for aluminum. Behler [5] suggested an additional quadratic term to describe the relationship more precisely. However, impurities in material and processing of the metal (warm or cold rolling of the copper wire) may cause significant variations. In consideration of those uncertainties any higher-order approximations seems questionable.

Combining Eqs. (2), (3) and (14) leads to the implicit relationship for the voice coil temperature

$$\Delta T_v = \frac{u^2 R_t}{Z_{\min}(T_a) + R_e(T_a)\delta \Delta T_v} \tag{15}$$

corresponding with the feedback loop as shown in Fig. 1. Solving this equation gives a nonlinear relationship between temperature

$$\Delta T_v \approx \frac{Z_{\min}(T_a)}{2\delta R_e(T_a)}\left(\sqrt{1 + \frac{4U^2 R_t \delta R_e(T_a)}{Z_{\min}(T_a)^2}} - 1\right). \tag{16}$$

and voltage $u$. Whereas the temperature is proportional to the squared voltage $u^2$, at lower values it rises only linearly with $u$ for $\Delta T_v > 250^o$ C. This effect gives some relief in the heating of the coil supposed the driver can handle such high temperatures.

Button [2] predicted the sound pressure level

$$SPL = \left(112 + 10\log(\eta_0(T_a)) - 10\log\left(\frac{R_t 1W}{\Delta T_v}(1 + \delta\Delta T_v)\right)\right)dB \tag{17}$$

as a function of the voice coil temperature $\Delta T_v$ using the efficiency $\eta_o(T_a)$ of the cold coil and constant parameters $R_t$ and $\delta$. Taking $\Delta T_v$ to infinity leads to the maximal SPL output

$$SPL_{\max} = (112 + 10\log(\eta_0(T_a)) - 10\log(R_t\delta \cdot 1W))dB \tag{18}$$

depending only on efficiency $\eta_o(T_a)$, the thermal resistance $R_t$ and the thermal coefficient of conductivity $\delta$. Thus, even a stimulus at extremely high voltage will only give a limited output under steady-state condition due to the compression of both input power and efficiency.

Referring the last term in Eq. (17) to the electrical input power of the cold driver $P_t(T_a) = U^2/Z_{\min}(T_a)$ and Eq. (5) gives the power compression factor

$$PC = 10\log\left(\frac{R_t P_t(T_a)}{\Delta T_v}(1 + \delta\Delta T_v)\right) = 10\log\left(\frac{P_t(T_a)}{P_t(T_v)}(1 + \delta\Delta T_v)\right) \tag{19}$$

$$= 10\log\left(\frac{Z_{\min}(T_v)U^2}{Z_{\min}(T_a)U^2}(1 + \delta\Delta T_v)\right) = 10\log\left((1 + \delta\Delta T_v)^2\right)$$

$$= 20\log(1 + \delta\Delta T_a)$$

which describes the reduction of output SPL level of a warm driver compared to a cold driver for the same voltage U. Thus, the power compression PC occurs due to the loss of half-space reference efficiency and to less drive from a constant voltage source into a rising impedance.

## 3.4   Limits of the Linear Modeling

Although the traditional modeling gives a lot of enlightening results, the thermal behavior of the real driver is much more complex when the spectral properties of the stimulus change. This is illustrated in a first experiment performed on example driver A. Three kinds of music interrupted

by a short break are used as stimulus. The increase of the voice coil temperature $\Delta T_v$ and the power $P_{Re}$ dissipated on resistance $R_e$ is recorded in Fig. 3.

Clearly, the voice coil temperature follows the power $P_{Re}$ approximately. In the breaks when no power is supplied to the coil, the temperature decays slowly to the ambient temperature. A large time constant is used for the integration of the power to compare the "mean" input power with the steady state temperature at three samples $t_1$, $t_2$ and $t_3$. Here the total thermal resistance is approximated by the ratio $\Delta T_v/P_{Re}$ and listed in Table 1.

Significant variation (60 %) are found in the measured thermal resistance depending on the properties of the signal. Apparently, the high bass content of the popular music gives much better cooling of the coil than a cappella singer program. This effect is very important but not considered in the traditional modeling. Thus, the parameters of the linear model have to be handled as effective parameters and are only valid for a particular stimulus. In order to compare the power handling special kinds of test noise have been defined by national and international committees (IEC 60268, EIA 426). However, it is questionable how these test signals represent contemporary popular music which almost always evolves more bass. As a second point, the thermal parameters measured on a driver may not applied to the same driver when mounted in a vented enclosure and operated via a crossover network.

To provide more meaningful parameters for the evaluation of drivers and for the design of passive and active loudspeaker systems the thermal modeling has to consider the following mechanisms:

- Dependence of input power on impedance response

- variation input impedance due to driver nonlinearities

- heating process due to eddy currents and magnetization

- cooling process due to forced air convection

- stalled convection cooling due to amplitude compression of displacement and velocity.

## 4  Nonlinear Modeling

Nonlinear modeling is a natural extension of the traditional modeling. The electro-mechanical system in Fig. 4 supplies the power $P_{Re}$, the power $P_{R2}$ dissipated in resistance $R_2$, displacement $x$ and velocity $v$ of the voice coil to the thermal model and the voice coil temperature $\Delta T_v$ is given back to the resistance $R_e$. The nonlinear effects in both systems are discussed separately in the following.

## 4.1  Electro-mechanical System

The electrical and mechanical state variables in the electro-mechanical system determine how much input power is converted to heat. The equivalent circuit depicted in Fig. 5 considers the dominant nonlinear mechanisms in electro-dynamical transducers caused by force factor $Bl(x)$, stiffness $K_{ms}(x)$ and inductance $L_e(x)$ depending on the voice coil displacement $x$.

Fig. 6 shows the *Bl(x)*-characteristic for speaker A. The curve is almost symmetrical revealing that the coil has the optimal rest position. Due to the limited height of the coil the force factor decays in a natural way for any positive or negative displacement. The stiffness as shown Fig. 7 increases for any displacement. The minor asymmetry may be caused by the geometry of the pot spider. The inductance in Fig. 8 has a distinct maximum at negative displacement which is typical for any driver without a shorting ring or copper cap on the pole piece. The nonlinear elements *R_2(x), L_2(x)* representing the para-inductance at higher frequencies have the same shape as curve *L_e(x)*. The nonlinear inductance also produces a reluctance force on the mechanical side which can be interpreted as a electro-magnetic motor force.

### 4.1.1  Dynamics of the Mechanical System

The behavior of the nonlinear system is investigated for a sinusoidal stimulus. Both the frequency and the amplitude are varied from 5 Hz to 1 kHz. The amplitude of the tone is also varied in four equal-spaced intervals. The measurement time is very short that the heating of the coil is negligible. Fig. 9 shows the resulting amplitude of the fundamental component of the voice coil displacement. Although the voltage is increased equally the resulting displacement rises at high amplitudes less than at smaller amplitudes. Thus, the driver nonlinearities cause also a compression of the output signal.

Fig. 10 shows the displacement response versus frequency for a constant excitation voltage. A laser triangulation sensor is used to measure the displacement of the diaphragm. The measured curve agrees very well with the predicted curve using the large signal model as shown in Fig. 5. The third curve represents the results of a linear model using the traditional small signal parameters. Clearly, the linear model fails and predicts twice the output of the real speaker at low frequencies. Fig. 11 also reveals a significant loss of velocity due to amplitude compression. This increases the voice-coil temperature via two ways:

First, the reduced back EMF will vary the electrical input impedance about the resonance frequency dramatically and will increase the electrical current and the input power $P_{Re}$ as shown in Fig. 12 and Fig. 13, respectively. At a frequency of 40 Hz the cold voice coil absorbs 10 times more power as predicted by the linear model.

Second, the amplitude compression stalls the convection cooling. Both effects may cause a significant increase in the voice coil temperature when increasing the signal amplitude. This is important for drivers operated close to the resonance frequency, as in subwoofer systems.

Fig. 14 shows the effect of the variation of the voice coil resistance ($\Delta T_v = 0$ K and $\Delta T_v = 100$ K) on the sound pressure response by using a linear and a more precise nonlinear model. If the sinusoidal tone $f_l$ is above the resonance frequency $f_s$ the linear and nonlinear models coincide, giving a power compression $PC = 2.9$ dB. The power compression decreases at higher frequencies where the inductance contributes significantly to the electrical impedance. Below the resonance frequency the nonlinear model reveals 8 dB less output due to the effect of the driver nonlinearities. However, voice coil heating causes here only half the thermal power compression predicted by a linear model.

Applying a two-tone signal or any other complex stimulus such as music to the driver there is also nonlinear amplitude compression at higher frequencies. Fig. 15 shows the amplitude

response of the first tone (voice tone) with variable frequency $f_1$ while a second tone (bass tone) at fixed frequency $f_2 = 20$ Hz with the same amplitude ($u = 8$V rms) produces significant voice coil displacement.

Clearly the linear model cannot show any interactions between the two tones. The frequency responses for the cold and warm coil, represented by dotted and dashed lines in Fig. 15, respectively, are identical with the responses in Fig. 14 measured with one tone only. The real speaker reproduces the voice tone at low and high frequencies significantly lower than predicted by the linear model. Only above the resonance the nonlinear compliance causes an increase of 2 dB output of the fundamental component. The thermal power compression is almost negligible for frequencies below resonance.

The effects generated by a two-tone stimulus illustrate the variety of symptoms generated by speaker nonlinearities producing not only harmonic and intermodulation distortion but having also a significant impact on the fundamental output.

## 4.2   Nonlinear Thermal Model

The extended thermal model as shown in Fig. 16 contains the same lumped elements $R_{tv}$, $C_{tv}$, $R_{tg}$, $C_{tg}$ and $R_{tm}$, $C_{tm}$ representing the voice coil, pole tips and magnet, respectively, as the linear model in Fig. 2. However, there is an additional branch connected in parallel to the resistance $R_{tv}$ and an additional power source $P_{eg}$. The forced convection cooling is modeled by the thermal capacity $C_{ta}$ and variable resistances $R_{tc}(v)$, $R_{ta}(x)$ and $R_{tt}(v)$ depending on the velocity $v$ and displacement $x$ of the coil. These elements make the thermal model nonlinear. The resistance $R_{tc}(v)$ describes the heat transfer from the coil's surface to the surrounding air particles. Although the air velocity in the gap causes the variation of $R_{tc}(v)$ it is more practical to refer on the rms-value of the cone velocity $v_{rms}$. After introducing a convection parameter $r_v$ the thermal resistance is modeled by

$$R_{tc}(v) = \frac{1}{v_{rms}r_v} . \tag{20}$$

Some of the heat of the air will directly be transferred to the pole tips and to the magnet via the resistance $R_{tt}(v)$ but most heat will be transferred by air exchange via resistor $R_{ta}(x)$ to the ambience. This parameter depends on the displacement $x$ and the geometry of the driver and is modeled by

$$R_{ta}(x) = \frac{1}{x_{rms}r_x} \tag{21}$$

using the rms-value of the voice coil displacement $x_{rms}$ and a convection parameter $r_x$.

At low frequencies the voice coil displacement ensures sufficient air exchange and the transfer of the heat to the pole pieces via resistor $R_{tt}$ can be neglected in most drivers. The capacity $C_{ta}$ of the air involved in convection cooling can be approximated by

$$C_{ta} \approx m_{air} \frac{kW \cdot s}{kg \cdot K} \tag{22}$$

where the equivalent air mass $m_{air}$ is in kg and $C_{ta}$ is in Ws/K.

The extended model also considers the heat generated by the eddy currents induced in the voice coil former, pole tips and the surface of the magnet close to the coil.

The power supplied to the voice coil

$$P_{coil} = P_{Re} + \alpha\, P_{R2} \tag{23}$$

is the sum of the power dissipated in resistance $R_e$ according to Eq. (1) and a fraction (power shifting factor $\alpha$) of the power

$$P_{R2} = R_2 i_2{}^2 \tag{24}$$

dissipated by current

$$i_2 = \frac{i}{\sqrt{1 + \left(\dfrac{R_2}{L_2\, 2\pi f}\right)^2}}. \tag{25}$$

in $R_2$. The remaining power

$$P_{eg} = (1 - \alpha) P_{R2} \tag{26}$$

is directly transferred to the pole tips and magnet surface. An important characteristic in the new thermal model is the bypass power factor

$$\gamma = \frac{P_{con} + P_{eg}}{P_{Re} + P_{R2}} \tag{27}$$

which describes the part of the input power which bypasses the resistance $R_{tv}$. The larger the bypass factor $\gamma$ the more heat is directly be transferred to the iron and the ambience but does not contribute to the heating of the coil.

## 5    Verification of the Model

To verify the new elements in the extended modeling, series of special measurements have been performed on a variety of drivers, and the agreement between measured and predicted behavior has been investigated:

### 5.1    Measurement Setup

The driver under test is excited by a multi-tone stimulus as shown in Fig. 17. A first tone at fixed frequency $f_2 = 2$ kHz is generated to heat the voice coil significantly. Since the resonance frequency of driver A is below 40 Hz the movement caused by this tone is negligible. The frequency $f_1$ of the second tone is varied during the test in 10 steps spaced logarithmically between 5 and 200 Hz. This signal has been supplied as an external stimulus to the power test module (PWT) of the Distortion Analyzer. The stimulus is switched with a cycle scheme having

an ON and OFF phase of 2 minutes each. A small pilot tone at $f_p = 1$ Hz frequency is added to the cycled stimulus to measure the voice coil resistance $R_e$ at very low frequencies close to dc. Such an ac pilot tone is more convenient than using an additional dc-component because this signal can be supplied via a normal ac-coupled power amplifier to the speaker. This technique also avoids any dc-offset of the coil.

## 5.2  Results

Fig.  18 shows the monitored rms-values of voltage and current at the speaker terminals versus measurement time $t$. Starting at 5 Hz the frequency $f_1$ is increased after completing an On/Off cycle. Whereas voltage is held constant at 17 $V_{rms}$ during the On-phase the current varies according to the resistance $R_e$.

Using the 1 Hz pilot tone, the resistance $R_e$ is calculated during the power test and shown versus time $t$ in Fig.  19.

The increase of voice coil temperature

$$\Delta T_v = \frac{1}{\delta}\left(\frac{R_e(T_v)}{R_e(T_A)} - 1\right)$$

(28)

is calculated from $R_e(T_v)$ by using $\delta = 0.0393$ K$^{-1}$ for the known copper coil and the initial resistance $R_e(T_a)$ at ambient temperature.

Fig.  20 shows the variation of voice coil temperature $\Delta T_v$ and the power $P_{Re}$ versus measurement time. In each OFF-phase when the power $P_{Re}$ is zero the voice coil temperature $\Delta T_v$ decreases rapidly to a value $\Delta T_{off}$ close to the steady-state magnet temperature $\Delta T_{mss}$. In each ON-phase the voice coil temperature $\Delta T_v$ approaches the maximal value $\Delta T_{on}$ close to the value $\Delta T_{vss}$ of the coil in steady-state condition. During the whole test the magnet gradually increases by about 10 K. To reduce the influence of the thermal dynamics caused by the capacities $C_{tv}$, $C_{tg}$ and $C_{tm}$ the maximal variation of the voice coil temperature $T_{step} = \Delta T_{on} - \Delta T_{off}$ and the power $P_{Re}$ is measured at the end of each cycle.

The ratio $T_{step}/P_{Re}$ as shown in Fig.  21 describes the parallel connection of $R_{tv}$ and the convection resistance $R_{tc} + R_{ta}$ versus frequency $f_1$. The thermal resistance reduces by about 30% at $f_1 = $ 40 Hz compared with very low or high frequencies.

The sum of both convection resistances can be separated from $R_{tc}$ by

$$\left(R_{tc} + R_{ta}\right) = \frac{1}{\dfrac{P_{Re}(f_1)}{T_{step}(f_1)} - \dfrac{1}{R_{tv}}}$$

(29)

where resistance $R_{tv} = T_{step}(f_2)/P_{Re}(f_2) = 6.2$ K/W of the voice coil is measured by using the high-frequency tone $f_2 = 2kHz$ only.

Fig. 22 shows the measured frequency response of $R_{tc} + R_{ta}$ versus frequency $f_1$. Clearly this resistance decreases when the amplitudes of velocity and displacement in Fig. 23 rise.

Using the measured displacement and velocity in Fig. 23 optimal estimates of the convection parameters $r_v = 0.30$ and $r_x = 300$ in Eqs. (20) and (21) are determined by fitting the predicted to the measured curve in Fig. 22. The agreement is quite reasonable. Fig. 24 shows the resistances $R_{tc}$ and $R_{ta}$ separately. Over the measured frequency range $R_{tc}$ is greater than $R_{ta}$ indicating that the velocity mainly determines the forced convection cooling. $R_{ta}$ rises only at high frequencies because the small displacement cannot give sufficient air exchange. In any case, the $R_{ta}$ alone cannot model the convection cooling because at low frequencies the air velocity close to the coil's surface is important, not the pumping effect due to high displacement. If the nonlinear model has to be simplified for practical reasons, it seems possible to neglect $R_{ta}$ and to use the velocity dependent resistance $R_{tv}$ only.

## 6   Measurement of Thermal Parameters

The technique using the two-tone signal has been proven useful for the verification of the model. In many practical applications a simplified model in Fig. 25 is sufficient to describe the dominant effects. The air convection cooling is only represented by the velocity dependent resistance $R_{tc}(v)$ while the other parameters $R_{ta}$, $R_{tt}$, and $C_{ta}$ are neglected because $R_{tv} > R_{ta}$ and $R_{tt} >> R_{tv}$ and the mass of air in the gap is small. The remaining parameters of the simplified model can be identified in shorter time using available equipment.

### 6.1   Performing the Measurements

The suggested method requires four measurements. In the first measurement the linear parameters $R_e(T_a)$, $L_2$ and $R_2$ are determined from the electrical impedance of the cold driver. Then three long term power tests are performed using a single tone as stimulus, which is adjusted to the following frequencies:

- $f_1 \approx 10\,f_s$ to measure voice-coil and magnet parameters

- $f_2 >> f_1$ to measure direct heat transfer

- $f_3 \approx 1.5\,f_s$ to measure convection parameters.

The single tone $f_1$ in the first power test is set in the middle of the frequency band where the air convection cooling is negligible. The tone $f_2$ in the second test is set as high as possible to measure the largest effect of the eddy currents. The tone $f_3$ in the last test is set close but not directly at the resonance frequency $f_s$ to supply sufficient power to the driver.

The stimulus is switched on and off by a fixed cycle scheme ($t_{on}$ = 25 min, $t_{off}$ = 5 min). The amplitude of the stimulus is adjusted to the particular driver to get sufficient heating while avoiding thermal or mechanical damage. The duration of the power test should be sufficiently long ($> 4\,\tau_m$) to bring the pole plates, magnet and frame in thermal equilibrium.

During the test the rms-value of the input current $i(t)$ and voice-coil resistance $R_e(t)$ is monitored and recorded with sufficient temporal resolution. For the third stimulus $f = f_3$ the rms-value $x_{rms}(f_3)$ of the voice coil displacement is also measured.

## 6.2   Reading Temperature Variations

After performing all three power tests the instantaneous voice coil temperature $\Delta T_v(t)$ is calculated by using Eq. (28) and the conductivity $\delta$ appropriate for the coil material. Fig. 26 shows the temperature $\Delta T_v(t)$ and power $P_{Re}$ during the first power test performed on example driver A.

In the last cycle of the test when the coil and magnet reached the thermal equilibrium the maximal voice coil temperature $\Delta T_{on}(f)$ is measured at the beginning of the OFF-phase $t_{s\_off}$ for $f = f_1, f_2$ and $f_3$ as shown for the first measurement in Fig. 27. The short time constant of the voice coil $\tau_v$ causes the rapid decay at the beginning of the OFF-phase. The larger time constant $\tau_m$ of the magnet/frame structure causes an additional decay starting at later times. To separate both processes, the early decay is approximated by a straight line and the crossing point with the minimal temperature in the OFF-phase gives the slope time $t_{slope}$. At approximately 5 times of $t_{slope}$ the voice coil comes close to the thermal equilibrium and the temperature $\Delta T_{off}(f) = \Delta T_V(t_{s\_off} + 5t_{slope})$ can be measured for $f = f_1, f_2$ and $f_3$.

## 6.3   Reading Time Constants

Considering the Off-cycle of the first test with tone $f_1$ and searching for the temperature

$$\Delta T_{tau\_v}(t_{tau\_v}) = \Delta T_{TV}(t_{s\_off} + \tau_v) \tag{30}$$
$$= 0.37 \ \Delta T_{on}(f_1) + 0.63 \ \Delta T_{off}(f_1)$$

gives the time $t_{tau\_v}$ as illustrated in Fig. 28 and the time constant of the voice coil is calculated by

$$\tau_v = t_{tau\_v} - t_{s\_off} . \tag{31}$$

Finally, the temperature threshold $\Delta T_{tau\_m}$ is calculated where the time constant of the magnet is elapsed

$$\Delta T_{tau\_m} = \Delta T_V(t_{start} + \tau_m) = \Delta T_{on} - 0.37 * \Delta T_{off} . \tag{32}$$

After reading the starting time $t_{start}$ and the time $\tau_{tau\_m}$ when the voice coil temperature is equal to $\Delta T_{tau\_m}$ the time constant

$$\tau_m = t_{tau\_m} - t_{start} \tag{33}$$

is calculated.

## 6.4   Parameter Calculation

Using the results of the previous measurements the thermal parameters can be calculated:

1. Power splitting coefficient

$$\alpha = -\frac{\varepsilon\, P_{\mathrm{Re}}(f_2) - P_{\mathrm{Re}}(f_1)}{\varepsilon\, P_{R2}(f_2) - P_{R2}(f_1)} \tag{34}$$

with the power dissipated in $R_e$ and $R_2$ according Eqs. (1) and (24) and the ratio of the temperature variations

$$\varepsilon = \frac{\Delta T_{on}(f_1) - \Delta T_{off}(f_1)}{\Delta T_{on}(f_2) - \Delta T_{off}(f_2)} \tag{35}$$

measured at frequencies $f_1$ and $f_2$.

2. Thermal resistance of the magnet/frame structure

$$R_{tm} = \frac{\Delta T_{off}(f_1)}{P_{\mathrm{Re}}(f_1) + P_{R2}(f_1)}\, \frac{t_{on} + t_{off}}{t_{on}} \tag{36}$$

considering the mean power averaged over one cycle.

3. Thermal resistance of the voice coil

$$R_{tv} = \frac{\Delta T_{on}(f_1) - \Delta T_{off}(f_1)}{P_{\mathrm{Re}}(f_1) + \alpha P_{R2}(f_1)}. \tag{37}$$

considering both power sources.

4. Thermal capacity of the voice coil

$$C_{TV} = \frac{\tau_{TV}}{R_{TV}}. \tag{38}$$

5. Thermal capacity of the magnet structure

$$C_{TM} = \frac{\tau_M}{R_{TM}}. \tag{39}$$

6. Thermal resistance due to convection cooling

$$R_{tc} = \frac{1}{\dfrac{P_{\mathrm{Re}}(f_3)}{\Delta T_{on}(f_3)} - \dfrac{1}{R_{tv} + R_{tm}}}. \tag{40}$$

7. Convection cooling parameter

$$r_c = \frac{1}{x_{rms}\, 2\pi f_3 R_{tc}}. \tag{41}$$

## 6.5   Example

The measurement technique is applied to example driver A and the thermal parameters are listed in Table 2.

Only a few parameters describe the thermal properties of the driver. Together with the nonlinear model, the heat transfer and the resulting temperatures of the coil and magnet can be predicted for  any input signal having different spectral properties.  This may be illustrated by the temperatures and powers during the three power tests as  listed in Table 3. At 80 Hz the voice coil temperature $\Delta T_{on}$ is significantly lower than at 1 kHz while almost the same input power $P_{Re}$ is dissipated in $R_e$. The reason is that half of the power ($\gamma = 60\ \%$)  dissipated in $R_e$ and $R_2$ flows directly into the convection cooling. Also at 16 kHz a significant part ($\gamma = 46\ \%$) of the input power is directly transferred to the pole tips and does not contribute to the heating of the coil.

## 7   Optimal Thermal Design

The thermal model and a measurement technique for the parameters make is possible to assess design choices to improve the heat transfer and to develop loudspeakers with higher power handling. There are many ways in the literature such as using magneto fluid in the gap and providing special vents for ventilation in the pole plate. Here the classical vent in the pole piece of example driver B as illustrated in Fig.  30 is discussed which is found on many drivers. The main purpose of this vent is to ventilate the space confined by dome, pole piece and voice coil former. This vent has an influence both on the electro-mechanical and on the thermal behavior of the driver.

Linear, nonlinear and thermal parameters have been measured of the original driver B with the open vent and on the modified driver with completely sealed vent.

Fig.  31 shows the electrical impedances of the driver with open and sealed vent and Table 4 shows the variation of the linear parameters measured before performing the power test. Most parameters ($R_e$, $L_e$, $L_2$, $R_2$, $M_{ms}$) stay almost constant. The mechanical stiffness $K_{ms}$ decreased by 10 % during the first power may be caused by mechanical fatigue. Without any vent the enclosed air is pressed by the movement of the dome through the gap and the spider. The friction of the air flow in the gap increases the mechanical losses significantly. This reduces the electrical impedance at $f_s$ and decreases the $Q_{ms}$ from 8.5 down to 2.4. Since the electrical damping $Q_{es} = 0.38$ dominates the total loss factor $Q_{ts} = 0.33$, the overall performance of the driver is not changed significantly. This is also valid in the large signal domain where the $Q_{ts}(x)$ varies with voice coil displacement $x$ due to the effect of the driver nonlinearites of Bl(x) and $C_{ms}$(x).  Fig. 32 reveals that $Q_{ts}(x)$ doubles for a moderate displacement $x_{peak} = 4$ mm whereas the difference caused by the driver modification is much smaller. Sealing the vent neither produced audible noise due to turbulences in the gap nor increased the nonlinearities of the compliance.

After measuring the linear and nonlinear parameters the thermal performance is investigated. Using the two-tone technique described above, the parameters $R_{tc}(v)$ and $R_{ta}(x)$ are measured on driver with and without sealed vent by having comparable amplitudes of the voice coil displacement. One tone at 2 kHz was used for heating while the second tone was varied between 5 Hz and 200 Hz to investigate the influence of the voice coil displacement.  For the vented and sealed case the predicted curves in Fig. 33 and Fig.  34, respectively,  agree very well with the

measured curves. However, the driver with the sealed vent has a significantly lower total resistance $R_{tc}(v) + R_{ta}(x)$.

The differences in the convection cooling become more obvious in Fig. 35 and Fig. 36 showing the thermal resistance $R_{tc}(v)$ and $R_{ta}(x)$, separately. The thermal resistance $R_{tc}(v)$ has a minimum at the resonance frequency $f_s$ where the cone velocity $v$ is maximal. However, the minimal $R_{tc}$ of the driver with the closed vent in Fig. 36 is only a quarter of the value measured with the open vent. Obviously, sealing of the vent removes the bypass of the air flow and forces all the air through the gap and increases the volume velocity at the coil's surface.

The resistance $R_{ta}(x)$ is also significantly higher in the original driver B with the unsealed vent corresponding with a poor air exchange in the gap.

The lower the resistances $R_{tc}(v)$ and $R_{ta}(x)$, the more power will bypass the voice coil. The power bypass factor $\gamma$ in Fig. 37 reveals that up to 50 % of the input power will not contribute to the heating of the coil in the modified driver with the sealed vent. The convection cooling in the original driver can transfer up to 17 % directly to the ambience.

In the particular example, sealing the vent would bring a significant benefit in power handling without causing significant changes of $Q_{ts}$ and $f_s$ and other unpleasant effects. However, this cannot be generalized for all drivers. If the diameter of the coil is large and the relative variation of the volume below the dust cap becomes high, the nonlinear compliance of the enclosed air may produce harmonic distortion. The asymmetrical characteristic may also generate a dc-component in the voice coil displacement, shifting the coil in a positive direction to the compliance maximum (away from the back-plate). A high velocity in the gap may also generate additional noise due to turbulences. Thus, vent's area $A_v$ should be as small as possible to exploit the convection cooling and as large as necessary to avoid the nonlinear effects.

## 8   Conclusion

In the large signal domain where the heating of the coil is a relevant issue, the driver nonlinearities $Bl(x)$, $C_{ms}(x)$ and $L_e(x)$ and forced air convection have a dramatic influence on the voice coil temperature $T_v$. Thus, a nonlinear model is required to consider the complicated interactions between electrical-mechanical and thermal mechanisms. An equivalent circuit with lumped elements having nonlinear parameters is introduced which is a natural extension of the traditional modeling. This model has been verified on multiple loudspeakers. The free parameters of the model can be identified for a particular driver by a simple technique also suggested in this paper.

This model allows a better prediction of the voice coil temperature and other state variables of the loudspeaker for any audio input. It can be easily implemented in a numerical simulation tool for loudspeaker design or in digital controllers.

The modeling, prediction and measurement give valuable insight in the heat transfer in loudspeakers:

The convection cooling and the direct heat transfer to the magnet/pole tips due to eddy currents are important bypasses reducing the heating of the coil. The fraction of power which does not

directly contribute to the heating of the coil can be expressed by the bypass factor $\gamma$. This parameter should be optimized in practical design.

The nonlinear parameters $Bl(x)$, $C_{ms}(x)$ and $L_e(x)$ vary the electrical input impedance and increase the input power of the speaker. The nonlinearities also cause a compression of the displacement amplitude which impairs the natural convection cooling. Both effects increase the voice coil temperature.

The most critical path in air convection cooling is the heat transfer between coil's surface and the air layer surrounding the coil. The resistance $R_{tc}(v)$ depends on the cone velocity $v$. Fortunately, high voice coil velocity $v$ coincides with sufficient voice coil displacement $x$ ensuring air exchange and the heat transfer to the ambience.

A precise loudspeaker model considering the nonlinear and thermal effects reveals the causes of signal distortion and the factors limiting mechanical displacement and power handling. The practical examples in this paper revealed the unused potential of common drivers which can be exploited for improvement of the large signal performance.

## 9    References

[1] Henricksen, "Heat Transfer Mechanisms in Loudspeakers: Analysis, Measurement and Design, " J. Audio Eng. Soc. Vol 35. No. 10 , 1987 October.

[2] D. Button, Heat Dissipation and Power Compression in Loudspeakers, J. Audio Eng. Soc., Vol. 40, No1/2 1992 January/February.

[3] C. Zuccatti, Thermal Parameters and Power Ratings of Loudspeakers, J. Audio Eng. Soc., Vol. 38, No. 1,2, 1990 January/February.

[4] P. J. Chapman, "Thermal Simulation of Loudspeakers," presented at the 104th Convention of Audio Eng. Soc., May 1998, Preprint 4667.

[5] G. Behler, A. Bernhard, "Measuring  Method to derive the Lumped Elements of the Loudspeaker Thermal Equivalent Circuit," presented at the 104th Convention of Audio Eng. Soc. 1998 May 16-19, Amsterdam, preprint #4744.

[6] G. Behler, "Measuring  the Loudspeaker's Impedance During Operation for the Derivation of the Voice Coil Termperature," presented at the 98th Convention of Audio Eng. Soc1995 February 25-28, Paris, preprint #4001.

[7] K. M. Pedersen, "Thermal Overload Protection of High Frequency Loudspeakers," Report of Final Year Dissertation at Salford University.

[8] "Measurement of Nonlinear Thermal Loudspeaker Parameters, " Application note AN19, KLIPPEL GmbH,  www.klippel.de.

Table 1: Total thermal resistance of driver A depending on the stimulus.

Table 2: Thermal parameters of the driver A

Table 3: Voice coil temperatures and power splitting depending on the frequency of the test tone.

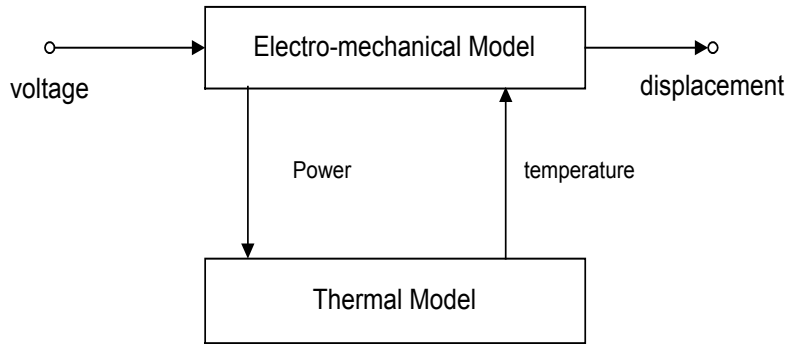Table 4: Linear parameters of the driver B with open and sealed vent and the rear pole plate.

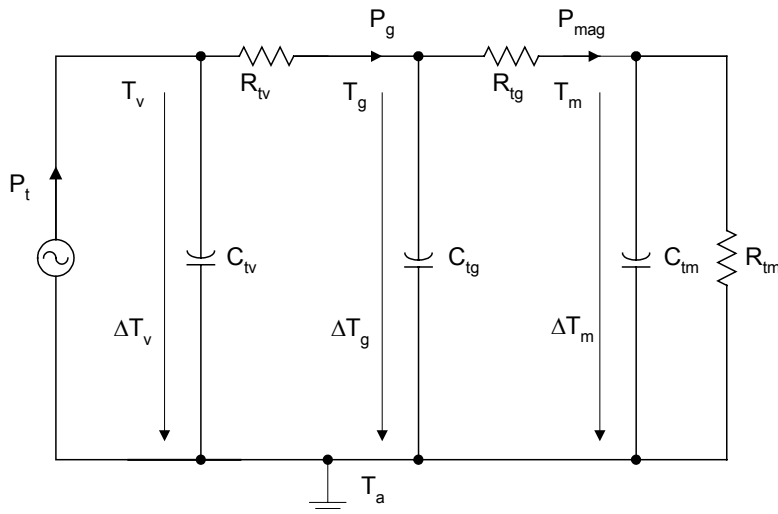Fig. 1: Interaction between the linear electro-mechanical and thermal model
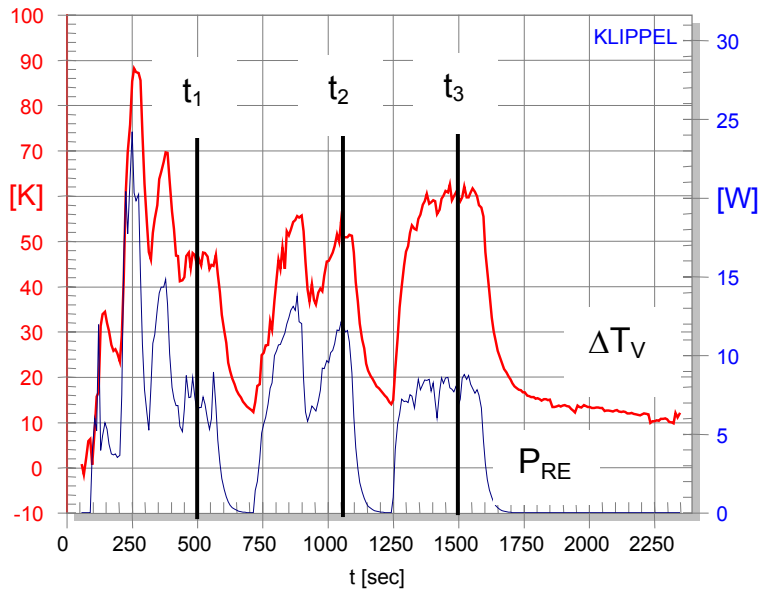
Fig. 2: Linear thermal model

Fig. 3: Voice coil temperature $\Delta T_v$ and power $P_{Re}$ versus time while reproducing different music material
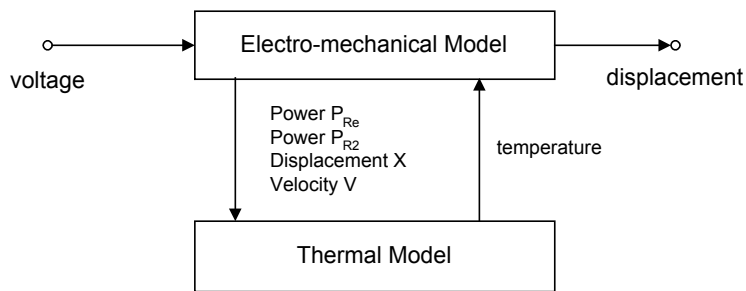
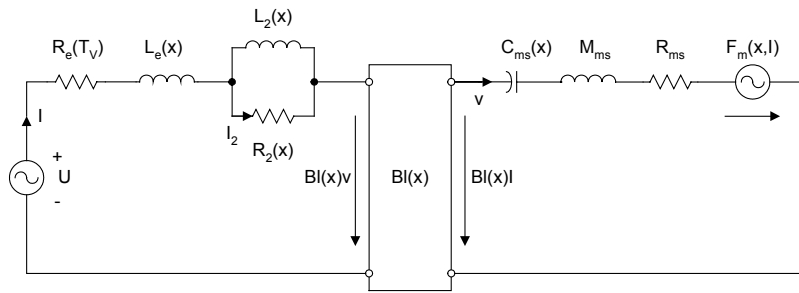Fig. 4: Interactions between the nonlinear models

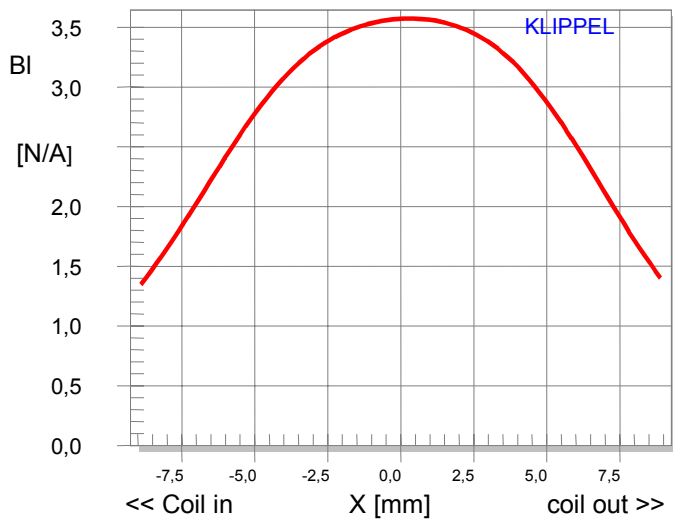Fig. 5: Lumped-Parameter Model for the electro-mechanical system

Fig. 6: Force factor $Bl(x)$ of driver A versus voice coil displacement $x$
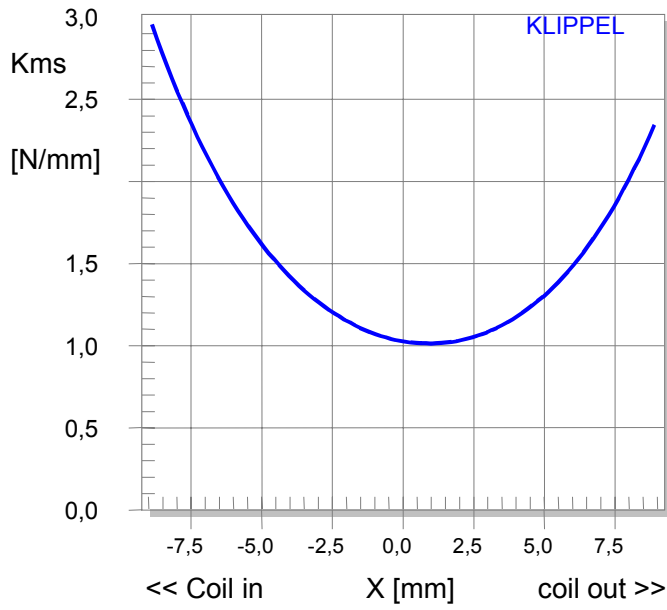
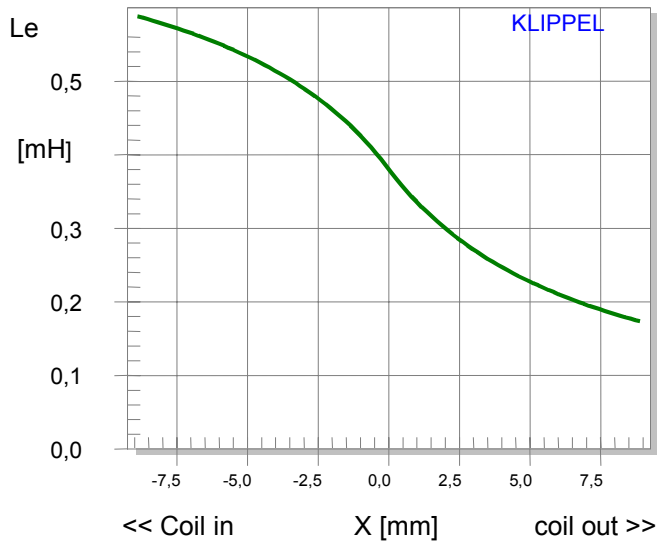Fig. 7: Stiffness $K_{ms}(x)$ of driver A versus displacement $x$

Fig. 8: Voice coil inductance $L_e(x)$ of driver A versus displacement $x$

Fig. 9: Voice coil displacement of driver A at ambience temperature for a sinusoidal excitation tone versus frequency $f_1$ and voltage $u_1$

Fig. 10: Voice coil displacement $x$ versus frequency $f_1$ of driver A at ambient temperature measured (dashed line) and calculated by using a linear model (thin line) and a nonlinear model (thick line).

Fig. 11: Voice coil velocity $v$ of driver A at ambient temperature calculated by a linear (thin line) and nonlinear (thick line) model versus frequency $f_1$

Fig. 12: Rms-value of the input current $i$ of driver A at ambient temperature calculated by a linear model (thin line) and a nonlinear model (thick line)

Fig. 13: Input power $P_{Re}$ of driver A at ambient temperature calculated by a linear and nonlinear model

Fig. 14: Sound pressure frequency response of the cold and warm coil predicted by linear and nonlinear model.

Fig. 15: Amplitude of fundamental sound pressure component versus frequency $f_1$ of a warm and cold driver excited by a two-tone stimulus ($f_1$ variable, $f_2 = 20$ Hz, $u_1 = u_2 = 8$ V$_{rms}$) predicted by a linear and nonlinear model.

Fig. 16: Nonlinear thermal model

Fig. 17: Measurement setup to measure convection cooling

Fig. 18: Voltage $u_{rms}$ (thin line) and current $I_{rms}$ (thick line) of the cycled two-tone signal ($f_2 =$ const., $f_1 =$ varied from 5 to 200 Hz) versus measurement time.

Fig. 19: dc voice coil resistance $R_e$ versus measurement time

Fig. 20: Voice coil temperature $\Delta T_v$ (thin line) and power $P_{Re}$ dissipated in resistance $R_e$ (thick line) versus measurement (varied frequency $f_1$)

Fig. 21: Increase of the voice coil temperature $T_{step}$ by providing an input power $P_{Re}$ during cycling

Fig. 22: Measured and predicted total resistance $R_{tv}+R_{ta}$ representing total convection cooling versus excitation frequency $f_1$

Fig. 23: Voice coil displacement $x_{rms}$ and velocity $v_{rms}$ versus frequency $f_1$

Fig. 24: Thermal resistance $R_{tc}(v)$ and $R_{ta}(x)$ versus frequency $f_1$ of the excitation signal

Fig. 25: Simplified thermal model

Fig. 26: Voice coil temperature $\Delta T_V$ (thin line) and Power $P_{Re}$ (thick line) of a cycled $f_1 = 1$ kHz tone versus time.

Fig. 27: Reading temperature $T_{on}$ and $T_{off}$ in the cooling phase of the last ON/OFF-cycle.

Fig. 28: Reading the time constant $\tau_v$ in the cooling phase

Fig. 29: Reading the time constant $\tau_m$ of the magnet.

Fig. 30: Sectional view of a driver with vented back plate

Fig. 31: Electrical input impedance of the original driver with open vent (thick line) and of the modified driver with sealed vent (thin line).

Fig. 32: Total loss factor $Q_{ts}(x)$ versus displacement $x$ considering nonlinearities of driver B with open or sealed vent.

Fig. 33: Measured and predicted total resistance $R_{tc}+R_{ta}$ of the original driver B with open vent

Fig. 34: Measured and predicted total resistance $R_{tc}+ R_{ta}$ of the modified driver B with sealed vent

Fig. 35: Thermal resistances $R_{tc}(v)$ and $R_{ta}(x)$ versus frequency $f_1$ of the original driver B with open vent

Fig. 36: Thermal resistances $R_{tc}(v)$ and $R_{ta}(x)$ versus frequency $f_1$ of the modified driver B with sealed vent

Fig. 37: Bypass power factor $\gamma$ versus frequency of the excitation tone for the driver with and without vent

| Sample | Music | Start [s] | $\Delta T_v$ [K] | $P_{Re}$ [W] | $\Delta T_v/P_{Re}$ [K/W] |
|--------|-------|-----------|------------------|--------------|---------------------------|
| $t_1$ | Violin concert | 0 | 48 | 7 | 6.8 |
| | Break | 600 | | | |
| $t_2$ | Popmusic | 700 | 52 | 11.5 | 4.6 |
| | Break | 1100 | | | |
| $t_3$ | Vocal Singer | 1250 | 60 | 8 | 7.5 |
| | Break | 1550 | | | |

Table 1: Total thermal resistance of driver A depending on the stimulus.

| Parameter | Value | Unit |
|-----------|-------|------|
| $R_{tv}$ | 5.9 | K/W |
| $C_{tv}$ | 3.6 | Ws/K |
| $m_{copper}$ | 9.7 | g |
| $R_{tm}$ | 4.1 | K/W |
| $C_{tm}$ | 272 | Ws/K |
| $m_{steel}$ | 545 | g |
| $r_v$ | 0.12 | $Ks^2/Wm^2$ |
| $\alpha$ | 36 | % |
| $R_e(T_a)$ | 1.88 | $\Omega$ |
| $R_2$ | 7.97 | $\Omega$ |
| $L_2$ | 0.23 | mH |
| $\delta$ | 0.00393 | $K^{-1}$ |

Table 2: Thermal parameters of the driver A

| Measurement | 1st | 2nd | 3rd | Unit |
|---|---|---|---|---|
| $f$ | 1000 | 16000 | 80 | Hz |
| $\Delta T_{on}$ | 138 | 130 | 52 | K |
| $\Delta T_{off}$ | 52 | 75 | 20 | K |
| $P_{Re}$ | 14 | 4.8 | 13 | W |
| $P_{coil}$ | 14.5 | 9.3 | 13 | W |
| $P_{eg}$ | 0.8 | 7.9 | 0 | W |
| $P_{R2}$ | 1.3 | 12.4 | $\approx 0$ | W |
| $P_{tv}$ | 14.6 | 9.3 | 5.2 | W |
| $P_{mag}$ | 15.4 | 17.2 | 5.3 | W |
| $P_{con}$ | $\approx 0$ | $\approx 0$ | 7.8 | W |
| $\gamma$ | 5.3 | 46 | 60 | % |

Table 3: Voice coil temperatures and power splitting depending on the frequency of the test tone.

| Parameters | Vent open | Vent sealed | unit |
|---|---|---|---|
| $R_e$ | 5.72 | 5.78 | Ohm |
| $L_e$ | 0.089 | 0.092 | mH |
| $L_2$ | 0.773 | 0.730 | mH |
| $R_2$ | 2.84 | 2.81 | Ohm |
| $f_s$ | 48.0 | 45.0 | Hz |
| $M_{ms}$ | 14.744 | 14.843 | g |
| $R_{ms}$ | 0.523 | 1.756 | kg/s |
| $C_{ms}$ | 0.75 | 0.84 | mm/N |
| $K_{ms}$ | 1.34 | 1.19 | N/mm |
| $Bl$ | 8.00 | 7.99 | N/A |

| | | | |
|---|---|---|---|
| Qms | 8.51 | 2.39 | |
| Qes | 0.40 | 0.38 | |
| Qts | 0.38 | 0.33 | |

Table 4: Linear parameters of the driver B with open and sealed vent and the rear pole plate.

Fig. 1: Interaction between the linear electro-mechanical and thermal model



Fig. 2: Linear thermal model

Fig. 3: Voice coil temperature $\Delta T_v$ and power $P_{Re}$ versus time while reproducing different music material



Fig. 4: Interactions between the nonlinear models

Fig. 5: Lumped-Parameter Model for the electro-mechanical system



Fig. 6: Force factor *Bl(x)* of driver A versus voice coil displacement *x*

Fig. 7: Stiffness $K_{ms}(x)$ of driver A versus displacement $x$



Fig. 8: Voice coil inductance $L_e(x)$ of driver A versus displacement $x$

Fig. 9: Voice coil displacement of driver A at ambience temperature for a sinusoidal excitation tone versus frequency $f_1$ and voltage $u_1$

Fig. 10: Voice coil displacement $x$ versus frequency $f_1$ of driver A at ambient temperature measured (dashed line) and calculated by using a linear model (thin line) and a nonlinear model (thick line).

Fig. 11: Voice coil velocity *v* of driver A at ambient temperature calculated by a linear (thin line) and nonlinear (thick line) model versus frequency $f_1$



Fig. 12: Rms-value of the input current *i* of driver A at ambient temperature calculated by a linear model (thin line) and a nonlinear model (thick line)

Fig. 13: Input power $P_{Re}$ of driver A at ambient temperature calculated by a linear and nonlinear model



Fig. 14: Sound pressure frequency response of the cold and warm coil predicted by linear and nonlinear model.

Fig. 15: Amplitude of fundamental sound pressure component versus frequency $f_1$ of a warm and cold driver excited by a two-tone stimulus ($f_1$ variable, $f_2 = 20$ Hz, $u_1 = u_2 = 8$ V$_{rms}$) predicted by a linear and nonlinear model.



Fig. 16: Nonlinear thermal model

Fig. 17: Measurement setup to measure convection cooling



Fig. 18: Voltage $u_{rms}$ (thin line) and current $I_{rms}$ (thick line) of the cycled two-tone signal ($f_2$ = const., $f_1$ = varied from 5 to 200 Hz) versus measurement time.

Fig. 19: dc voice coil resistance $R_e$ versus measurement time



Fig. 20: Voice coil temperature $\Delta T_v$ (thin line) and power $P_{Re}$ dissipated in resistance $R_e$ (thick line) versus measurement (varied frequency $f_l$)

Fig. 21: Increase of the voice coil temperature $T_{step}$ by providing an input power $P_{Re}$ during cycling



Fig. 22: Measured and predicted total resistance $R_{tv}+R_{ta}$ representing total convection cooling versus excitation frequency $f_1$

Fig. 23: Voice coil displacement $x_{rms}$ and velocity $v_{rms}$ versus frequency $f_1$



Fig. 24: Thermal resistance $R_{tc}(v)$ and $R_{ta}(x)$ versus frequency $f_1$ of the excitation signal

Fig. 25: Simplified thermal model



Fig. 26: Voice coil temperature $\Delta T_V$ (thin line) and Power $P_{Re}$ (thick line) of a cycled $f_1 = 1$ kHz tone versus time.

Fig. 27: Reading temperature $T_{on}$ and $T_{off}$ in the cooling phase of the last ON/OFF-cycle.



Fig. 28: Reading the time constant $\tau_v$ in the cooling phase

Fig.  29: Reading the time constant $\tau_m$ of the magnet.



Fig.  30: Sectional view of a driver with vented back plate

Fig. 31: Electrical input impedance of the original driver with open vent (thick line) and of the modified driver with sealed vent (thin line).



Fig. 32: Total loss factor $Q_{ts}(x)$ versus displacement $x$ considering nonlinearities of driver B with open or sealed vent.

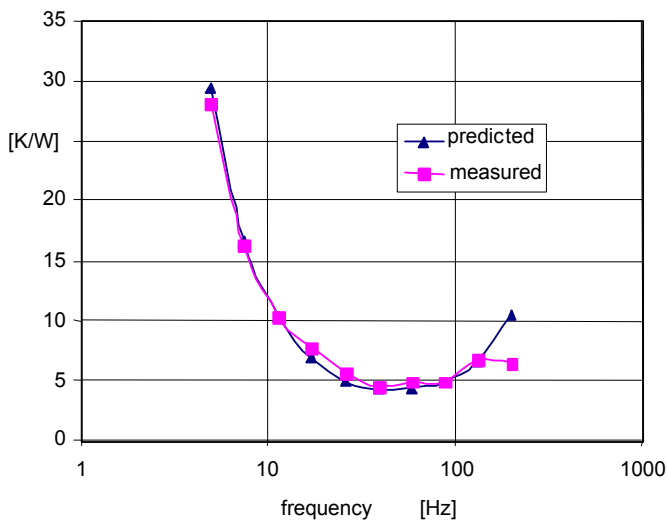Fig. 33: Measured and predicted total resistance $R_{tc}+R_{ta}$ of the original driver B with open vent



Fig. 34: Measured and predicted total resistance $R_{tc}+ R_{ta}$ of the modified driver B with sealed vent
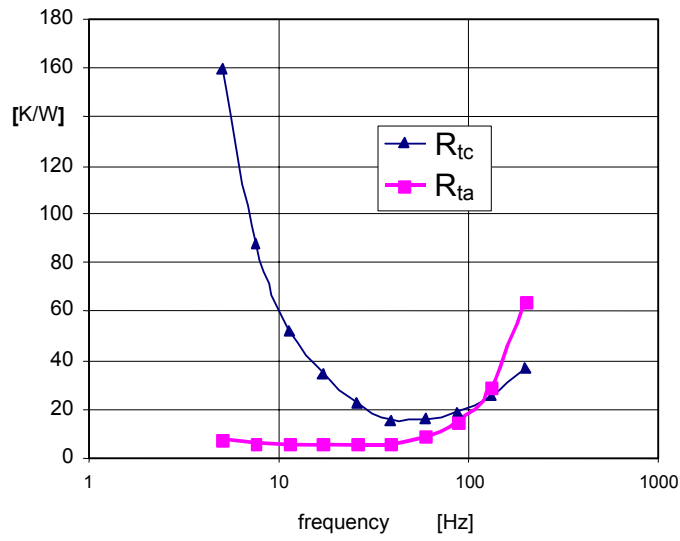
Fig. 35: Thermal resistances $R_{tc}(v)$ and $R_{ta}(x)$ versus frequency $f_1$ of the original driver B with open vent
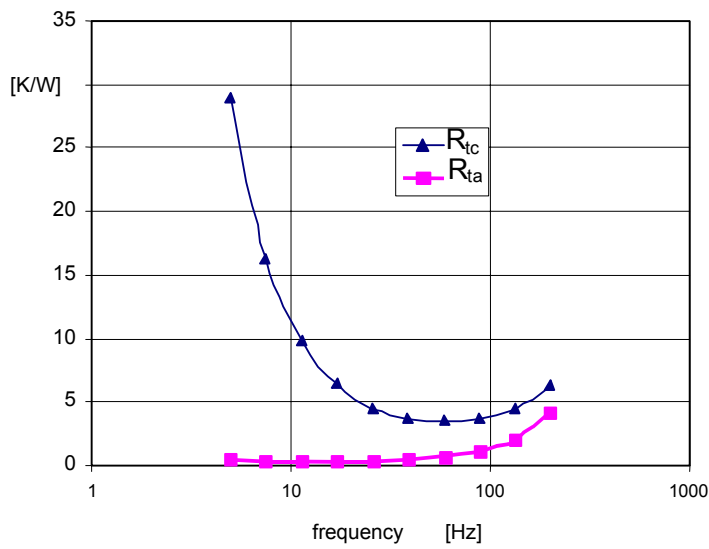


Fig. 36: Thermal resistances $R_{tc}(v)$ and $R_{ta}(x)$ versus frequency $f_1$ of the modified driver B with sealed vent
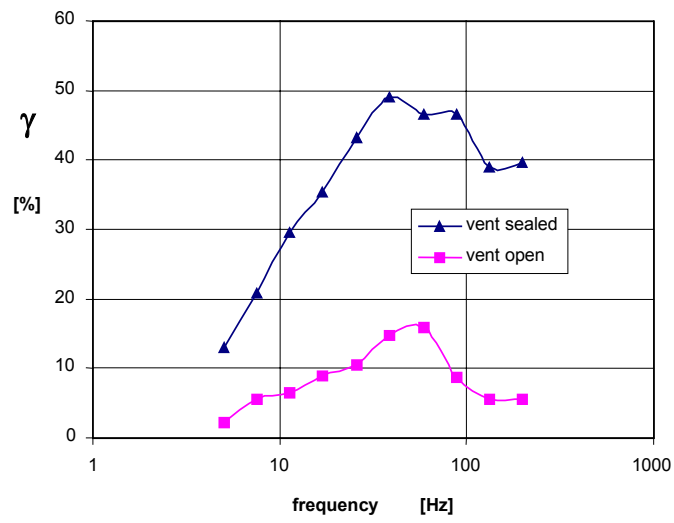
Fig. 37: Bypass power factor $\gamma$ versus frequency of the excitation tone for the driver with and without vent